Near-infrared emission line diagnostics for AGN from the local Universe to z ~ 3

Calabrò et al. 2023, arXiv:2306.08605, A&A accepted

Optical rest-frame spectroscopic diagnostics are usually employed to distinguish between star formation and AGN-powered emission. However, this method is biased against dusty sources, hampering a complete census of the AGN population across cosmic epochs. To mitigate this effect, it is crucial to observe at longer wavelengths in the rest-frame near-infrared (near-IR), which is less affected by dust attenuation and can thus provide a better description of the intrinsic properties of galaxies. AGN diagnostics in this regime have not been fully exploited so far, due to the scarcity of near-infrared observations of both AGNs and star-forming galaxies, especially at redshifts higher than 0.5. Using Cloudy photoionization models, we identify new AGN - star formation diagnostics based on the ratio of bright near-infrared emission lines, namely [SIII] 9530Å, [CI] 9850Å, [PII] 1.188μm, [FeII] 1.257μm, and [FeII] 1.64μm to Paschen lines (either Paγ or Paβ), providing simple, analytical classification criteria. We apply these diagnostics to a sample of 64 star-forming galaxies and AGNs at $0 \leq z \leq 1$, and 65 sources at $1 \leq z \leq 3$ recently observed with JWST-NIRSpec in CEERS. We find that the classification inferred from the near-infrared is broadly consistent with the optical one based on the BPT and the [SII]/Hα ratio. However, in the near-infrared, we find ~ 60% more AGNs than in the optical (13 instead of 8), with 5 sources classified as 'hidden' AGNs, showing a larger AGN contribution at longer wavelengths, possibly due to the presence of optically thick dust. The diagnostics we present provide a promising tool to find and characterize AGNs from $z = 0$ to $z \simeq 3$ with low and medium-resolution near-IR spectrographs in future surveys.

これまでは主にrest-opticalの輝線によって、AGN診断が行われてきた
but... 可視で隠されたAGNを多く見逃している可能性
- 理論研究では観測の最大一桁大きなblack-hole accretion rate density
→ rest-NIRでの診断図をCloudyで検討。特に明るい輝線によるもの。
→ 近傍の銀河とJWSTで観測された1<z<3の銀河に適応。

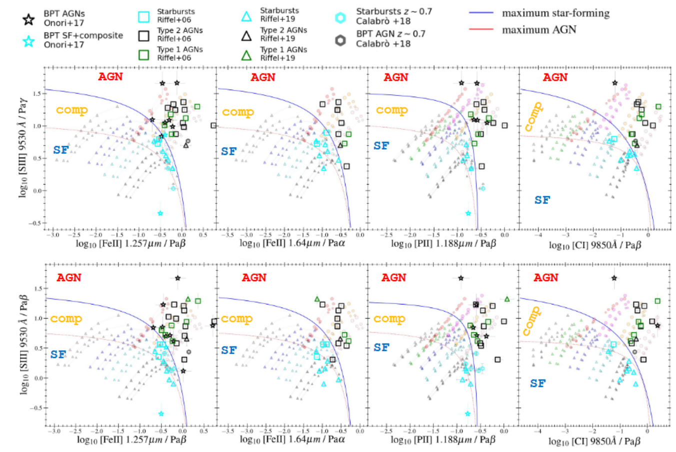

Fig. 9. Figures displaying the location of local and intermediate redshift AGNs and starbursts in the near-IR diagnostics defined in the paper: the Fe2S3-β, Fe2S3-α, P2S3, and C1S3 diagrams from left to right, as a function of [S III]/Paγ on the y-axis (*top row*) or [S III]/Paβ (*bottom row*). Sources coming from Riffel et al. (2006) and Riffel et al. (2019) are drawn with square symbols and triangles, respectively. Those presented and measured by Onori et al. (2017) are identified with empty stars, while starbursts from Calabrò et al. (2019) are shown with cyan hexagons. The underlying models are the same as described in Fig. 8.

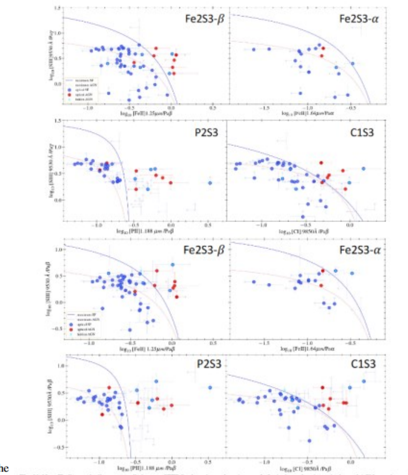

Fig. 11. Near-IR diagnostic diagrams applied to our CEERS selected sample at $1 < z < 3$. Optical star-forming galaxies and AGNs are drawn with blue and red circles, respectively. Hidden AGNs (i.e., optical star-forming but near-IR AGN) are identified as cyan crosses. Optical star-forming galaxies with upper limits are drawn without symbols in blue if their line ratios are still consistent with being star-forming. The red dashed and blue continuous lines represent the maximum AGN and starburst limits (respectively) according to our models. The analytical form of the separation lines is described in Equation 1, using the coefficients listed in Table 3.

Cloudyによるシミュレーション (pyCloudy)

- Star-forming: BPASS
- AGN: Cloudyの基本機能AGN

Star-forming models

SFH	log(U)	log n_H/cm^{-3}	Z_{gas} and Z_{stars} [$Z_\odot$]
constant, with age = 10^8 yr	−4,−3.5,−3, −2.5,−2, −1.5,−1	2, 3, 4	0.05, 0.1, 0.15, 0.2, 0.3, 0.4, 0.5, 0.7, 1, 2

AGN models (Risaliti et al. 2000)

T_{BB} [K]	α index	log(U)	log n_H/cm^{-3}	Z_{gas} [$Z_\odot$]
10^6	−1.2,−1.4, −1.7,−2.0	−4,−3.5,−3, −2,−1	2, 3, 4	0.3, 0.4, 0.5, 0.7, 1, 2, 3

4 x 2種類の新しい診断図

X軸

- [FeII]1.257um/Paβ: 金属量↗ → 輝線比↗、log(U)↗ → 輝線比 ↘
- [FeII]1.64um/Paα: より長い波長
- [PII]1.188um/Paβ: [FeII]よりless sensitiveだが、金属量に感度あり
- [CI]9850um/Paβ: log(U)↘ → 輝線比↗

Y軸

- [SIII]9530A/Paγ: 金属量↗ → 輝線比↗だが、$Z_\odot$でturning point、log(U)↗ → 輝線比 ↗だが、log(U)=-2でサチる(より高階電離)
- [SIII]9530A/Paβ: Paγが暗いので、Paβ版も作成

→ それぞれ解析的な境界線を定義(論文中Table 3)

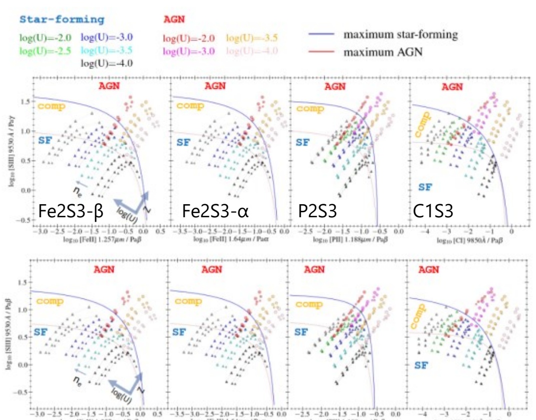

Fig. 8. Figure showing the near-IR diagnostic diagrams analyzed in this paper: Top row: [S III]/Paγ as a function of [Fe II]/Paβ (Fe2S3-β), [Fe II]/Paα (Fe2S3-α), [P II]/Paβ (P2S3), and [C I]/Paβ (C1S3). AGN models are represented as circles, colored as a function of log(U), and with sizes increasing with density. Star-forming models are the triangle symbols. The maximum AGN line and the maximum starburst separation limit are defined by a dotted red line and a continuous blue line, respectively. Bottom row: Same as above but as a function of the [S III]/Paβ line ratio on the y-axis.

観測データへの適応

0<z<1のlocal天体

- Magellan/FIRE starburst galaxies: 6天体
- 58 sources from literature(Riffel+2006,2019, Onori+2017)
  14 type1 AGN, 26 type2 AGN, 13 Starburst, 3 LINER, 5 mix

→ 可視の分類と矛盾ない。SFが高金属量に寄るのはサンプルがdustyなSBばかりだから。AGNもSFもlog(U)低めの領域に集まる。

1<z<3の天体

- JWST/NIRSpec MSA分光 (CEERS): 65天体
  - Hβ+[OIII] tripletからPβ+[FeII] tripletまでを最低限カバー
  - Hα+[NII] triplet と[SIII] 9530Aも同定

→ 可視の分類とおおよそ矛盾ない。P2S3やC1S3の方がはっきり分かれている。
(輝線が暗くて検出難しい。Opt-AGNはほとんど検出)。
5天体はOpt-SFでNIR-AGN
→ 可視ではダストに埋もれていたAGN

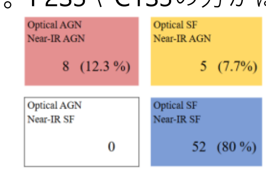

Fig. 12. Summary of the AGN and star-forming galaxy classification obtained from the rest-frame optical and near-IR spectroscopic diagnostics for the sample of 65 sources selected in CEERS.

Shockの判別

Mexican Million Models database (Morriset+2015)によるprediction
→ rest-NIR診断だとAGNと区別できる

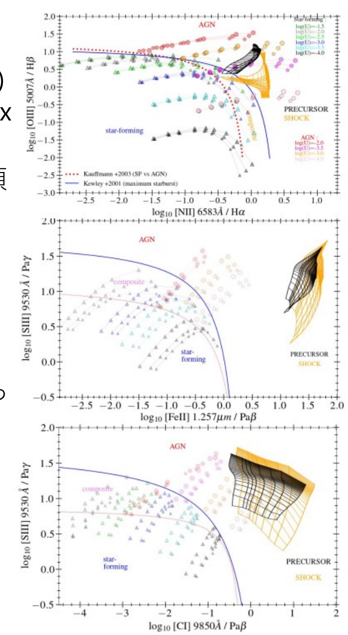

Fig. 13. Predictions of the shock models described in the text for the BPT diagram, the Fe2S3-β, and the C1S3 diagrams, from top to bottom. The AGN and SF models from Cloudy and the separation lines are the same as in Fig. 8.

今後の分光、面分光サーベイで活用